Current Optics and Photonics
Vol. 4, No. 6, December 2020, pp. 524-529

ISSN: 2508-7266(Print) / ISSN: 2508-7274(Online)
DOI: https://doi.org/10.3807/COPP.2020.4.6.524

Depth-fused-type Three-dimensional Near-eye Display Using a Birefringent Lens Set

Hogil Baek and Sung-Wook Min*

Department of Information Display, Kyung Hee University, Seoul 02447, Korea

(Received August 31, 2020 : revised October 20, 2020 : accepted October 26, 2020)

We propose a depth-fused-type three-dimensional (3D) near-eye display implemented using a birefringent lens set that is made of calcite. By using a birefringent lens and image source (28.70 mm × 21.52 mm), which has different focal lengths according to the polarization state of the incident light, the proposed system can present depth-fused three-dimensional images at 4.6 degrees of field of view (FOV) within 1.6 Diopter (D) to 0.4 D, depending on the polarization distributed depth map. The proposed method can be applied to near-eye displays like head-mounted display systems, for a more natural 3D image without vergence-accommodation conflict.

Keywords : Birefringence, Near-eye display, Depth-fused display
OCIS codes : (080.2730) Matrix method in paraxial optics; (110.4190) Multiple imaging

I. INTRODUCTION

Recently, as interest in and demands of augmented and virtual reality (AR/VR) have increased significantly, research and development of various kinds of near-eye displays (NEDs) have been actively pursued [1-5]. The main issues of an NED are not only the specification problems such as pixel size, resolution, and field of view (FOV) of the device, but also methodological topics such as providing natural depth sensing. The stereoscopic method was once taken for granted as the 3D display method for NEDs. In recent years, however, research about 3D display systems that can avoid 3D nausea caused by vergence-accommodation conflict and provide more natural 3D images has progressed [6, 7]. Nevertheless, most methods are not suitable for NEDs due to bulkiness and complication [8]. Therefore, the development of a simple, straightforward 3D display method for NEDs is essential for AR/VR display. The depth-fused (DF) display, a type of multifocal-plane 3D display satisfying accommodation cues, has advantages in realizing an NED because it can express continuous depth using only two layers, depending on the intensity distribution of layers according to the depth-fused effect [9, 10], and yields the 3D image relatively simply, using only the 2D image and depth map. A DF system using a polarization-distributed depth-map (PDDM), where each polarization state of the pixels is modulated depending on the depth information, was proposed; it was constructed using two layers of polarization-dependent diffuser [11]. Research was performed to increase the 3D volume by using more than three diffuser layers; in this case, however, the reconstructed image was severely blurred due to the interference of layers [12, 13]. In this paper, we propose a DF method using a birefringent lens set, which has two different focal lengths according to the incident polarization states. Although studies using birefringence have been conducted previously [14-18], we formulate the conditions under which the FOVs of the near and far virtual images coincide simply as the optical matrix. When applied to an NED system, the eyepiece lens set made with birefringence can represent two image planes without diffuser layers. The PDDM can also be applied to the proposed system directly, without any modification. We introduce the design rule for the birefringent eyepiece to match the images of the far and near planes with the same FOV, which makes the two images in the different planes appear as a single, overlapped image located somewhere between the two layers. The assembled eyepiece consists of convex and concave birefringent lenses. This research presents the specifications and experimental results for the proposed DF-type 3D NED system.

*Corresponding author: mins@khu.ac.kr, ORCID 0000-0003-4794-356X

Color versions of one or more of the figures in this paper are available online.

II. METHODS

The optical design of a NED can be classified into non-pupil-forming and pupil-forming types, depending on whether an intermediary image is formed. The non-pupil-forming system has some advantages, which are the fact that one is relatively free to set the pupil position, and a simple design with a small form factor. Thus the proposed design rule for the birefringent eyepiece is based on the non-pupil-forming type.

Figure 1 shows the scheme and design variables of the proposed optical system. The bifocal lenses have two different image planes, due to the effective focal length, which can be calculated using the lens specifications such as the radii of curvature and refractive indices, and system parameters such as the distances between the lenses. The bifocal lenses can be produced using a birefringent material, which has different refractive indices depending on the polarization state. Among the birefringent materials, calcite has the advantage of low chromatic aberration, because it has a relatively uniform refractive index for wavelengths in the visible-light region. Also, since the Abbe-number standard for spectacle lenses produced in South Korea is above 31 on average, it can be said that calcite (79.17 for extraordinary, 49.91 for ordinary) has fewer problems with chromatic aberration.

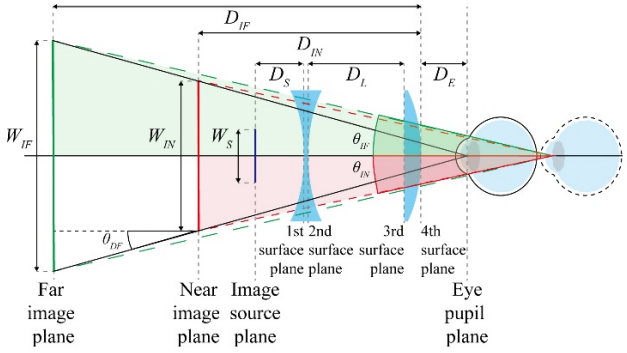

FIG. 1. The scheme of the proposed eyepiece using bifocal lenses. D_L represents the vertex distance between the lenses, and D_S represents the vertex distance from the first surface of the lens set to the image source. D_E represents the eye relief, the vertex distance from the last surface of the lenses to the eye. W_S is the diagonal length of the image source.

TABLE 1. Birefringent lens made of calcite

Lens shape	BI-Concave		Plano-Convex	
Center thickness (mm)	t_1		t_2	
	3.0		12.5	
Radius of curvature (mm)	R_1	R_2	R_3	R_4
	-73.3	+73.3	Infinity	-73.3
Refractive index (~590 nm)	n_o	n_e	n_o	n_e
	1.6581	1.4860	1.6581	1.4860
Focal length (mm)	-55.2	-74.9	+111.3	+150.8

Table 1 shows the specifications of the bifocal lenses used in our proposed system, which are made of calcite. Using the specifications of the birefringent lenses in Table 1, the ray-transfer matrix of the lens system in Fig. 1 can be calculated as follows:

$$
\begin{aligned}
M_{Lens} &= \begin{bmatrix} 1 & 0 \\ \frac{n-1}{R_4} & n \end{bmatrix}\begin{bmatrix} 1 & t_2 \\ 0 & 1 \end{bmatrix}\begin{bmatrix} 1 & 0 \\ \frac{1-n}{nR_3} & \frac{1}{n} \end{bmatrix}\begin{bmatrix} 1 & D_L \\ 0 & 1 \end{bmatrix}\begin{bmatrix} 1 & 0 \\ \frac{n-1}{R_2} & n \end{bmatrix}\begin{bmatrix} 1 & t_1 \\ 0 & 1 \end{bmatrix}\begin{bmatrix} 1 & 0 \\ \frac{1-n}{nR_1} & \frac{1}{n} \end{bmatrix} \\
&= \begin{bmatrix} \mathbf{A} & \mathbf{B} \\ \mathbf{C} & \mathbf{D} \end{bmatrix}, \\
\mathbf{A} &= \left\{ D_L\left[\frac{t_2(1-n)}{nR_3}+1\right]+\frac{t_2}{n}\right\}\left[\frac{1-n}{R_1}-\frac{1-n}{R_2}-\frac{t_1(1-n)^2}{nR_1R_2}\right] \\
&\quad +\frac{t_1(1-n)}{nR_1}+\frac{t_2(1-n)}{nR_3}+\frac{t_1t_2(1-n)^2}{n^2R_1R_3}+1, \\
\mathbf{B} &= \left\{ D_L\left[\frac{t_2(1-n)}{nR_3}+1\right]+\frac{t_2}{n}\right\}\left[1-\frac{t_1(1-n)}{nR_2}\right]+\frac{t_1t_2(1-n)}{n^2R_3}+\frac{t_1}{n}, \\
\mathbf{C} &= \left\{ D_L\left[\frac{1-n}{R_3}-\frac{1-n}{R_4}-\frac{t_2(1-n)^2}{nR_3R_4}\right]-\frac{t_2(1-n)}{nR_4}+1\right\}\left[\frac{1-n}{R_1}-\frac{1-n}{R_2}-\frac{t_1(1-n)^2}{nR_1R_2}\right] \\
&\quad +\left[\frac{1-n}{R_3}-\frac{1-n}{R_4}-\frac{t_2(1-n)^2}{nR_3R_4}\right]\left[\frac{t_1(1-n)}{nR_1}+1\right], \\
\mathbf{D} &= \left\{ D_L\left[\frac{1-n}{R_3}-\frac{1-n}{R_4}-\frac{t_2(1-n)^2}{nR_3R_4}\right]-\frac{t_2(1-n)}{nR_4}+1\right\}\left[1-\frac{t_1(1-n)}{nR_2}\right] \\
&\quad +\frac{t_1(1-n)}{nR_3}-\frac{t_1(1-n)}{nR_4}-\frac{t_1t_2(1-n)^2}{nR_3R_4},
\end{aligned}
\tag{1}
$$

where n is the refractive index, which is either n_o or n_e when the optical axes of the birefringent lenses are aligned the same, and D_L is the distance between the lenses. The distance to the image plane D_I indicates the locations of the virtual images that can be obtained using the ray-transfer matrix and the distance to the image source D_S. D_I depends on the refractive index and can be calculated by Eq. (2). In the proposed system D_I has a negative value, because a virtual image must be presented. According to n_o and n_e, as shown in Fig. 1, the farther value of D_I is D_{IF}, and the closer one is D_{IN}.

$$
\begin{aligned}
&D_I(n) = \frac{-1-\mathbf{A}(D_S\times\mathbf{C}-\mathbf{D})}{\mathbf{C}(D_S\times\mathbf{C}-\mathbf{D})}, \text{ where } D_I<0, \\
&D_{IF} = D_I(n_o), \text{ and } D_{IN} = D_I(n_e), \text{ when } |D_I(n_o)|>|D_I(n_e)|, \\
&D_{IF} = D_I(n_e), \text{ and } D_{IN} = D_I(n_o), \text{ when } |D_I(n_o)|<|D_I(n_e)|.
\end{aligned}
\tag{2}
$$

The diagonal length of the virtual image W_I can be obtained using the diagonal length of the image source and the distance to the image plane, as in Eq. (3):

$$W_I(n) = \frac{-W_S}{D_S \times \mathbf{C} - \mathbf{D}}, \text{ when } |W_{IF}| > |W_{IN}|,$$
$$W_{IF} = W_I(n_o), \text{ and } W_{IN} = W_I(n_e), \text{ for } |D_I(n_o)| > |D_I(n_e)|, \quad (3)$$
$$W_{IF} = W_I(n_e), \text{ and } W_{IN} = W_I(n_o), \text{ for } |D_I(n_o)| < |D_I(n_e)|.$$

To realize the DF system, the images in the near and far image planes should be matched. The two images do not match at the eye position indicated by the dotted outline in Fig. 1. In other words, the FOVs of the two image planes must be the same, and θ_{IF} must equal θ_{IN} in Fig. 1. The condition for the same FOV is shown in Eq. (4), where θ_{DF} is half of the FOV of the DF condition:

$$FOV_{DF} = 2\theta_{DF} = 2\tan^{-1}\left[\frac{W_{IF} - W_{IN}}{2\left(D_{IF} - D_{IN}\right)}\right]. \quad (4)$$

The position of the pupil for the DF condition, D_E, can be calculated using Eq. (5), where D_E should have a positive value to position the pupil outside of the eyepiece:

$$D_E = \frac{1}{D_S \times \mathbf{C} - \mathbf{D}}\left[\frac{W_S}{2\tan\left(\theta_{DF}\right)} - \frac{1}{\mathbf{C}}\right] - \frac{\mathbf{A}}{\mathbf{C}}, \text{ where } D_E > 0. \quad (5)$$

The depth range, which is the space from the near image plane to the far image plane, and proper eye relief should be considered under the DF condition. Because all terms of the transfer matrix in Eq. (1) are functions of D_L, FOV_{DF} and D_E are also functions of D_S and D_L. The other variables, such as the refractive indices and the radii of curvature, are fixed or hard to change once the bifocal lenses have been made. On the other hand, D_S and D_L can be easily changed and set as designed. Figure 2 shows the results of a simulation when constructing the birefringent lens set using the two calcite lenses of Table 1. The birefringent lens set is combined with a retrofocus structure to have the advantage of eye relief, compared to EFL. The horizontal axis of each graph represents D_L, and the vertical axis indicates D_s.

Figure 2(a) shows the FOV_{DF} conditions represented by Eq. (4), when the birefringent lens set with W_S of 35.9 mm present virtual images depending on the D_S values. Figure 2(b) shows the depth range of the images under the DF conditions. The depth range to design the experimental setup is set to 1875 mm, as indicated by the solid black line in the graph. Figure 2(c) show the values of D_E, which is set to 90.5 mm (as shown by the solid black line) in the proposed system to sufficiently include the folding mirror for the AR system. The black dashed lines in (a), (b), and (c) show D_E set to 90.5 mm and depth range set to 1875 mm respectively. At the intersection of

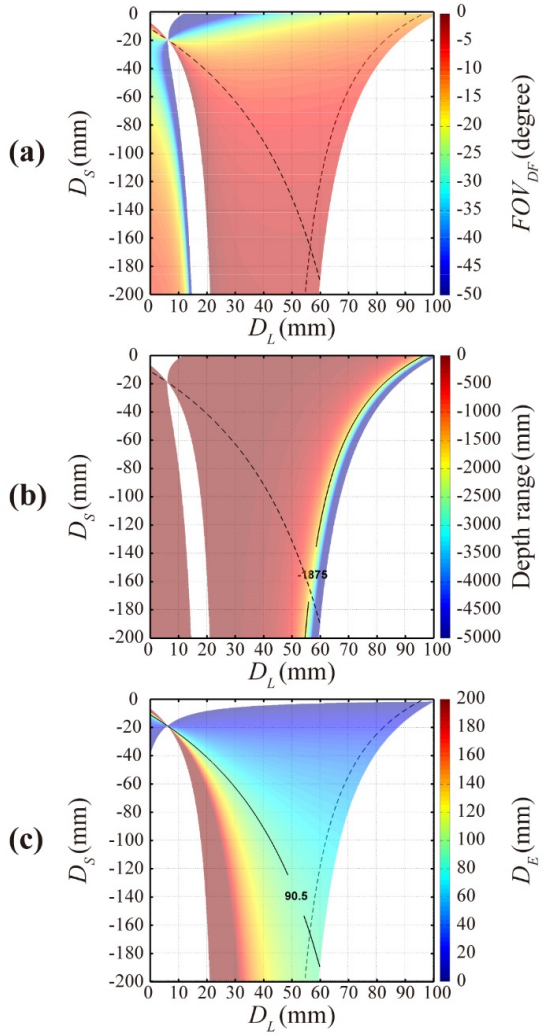

FIG. 2. Paraxial-ray-simulation results for the proposed system: (a) shows the FOV_{DF} conditions, (b) shows the depth range under the DF conditions, and (c) shows D_E under the DF conditions.

the two conditional settings, the value of FOV_{DF} is 4.6 degrees, the value of D_S is 166.3 mm, and the value of D_L is 56.5 mm, which is the designed value for the proposed system. However, this method has limitations on the degrees of freedom for designing the hardware. For example, when the optical components and eye-relief value are specified, the FOV is determined according to the chosen depth range. In other words, through Fig. 2 it is possible to derive the optimum state for the form factor, depth range, and position of the image to be implemented within the desired system configuration.

III. RESULTS

Figure 3 shows the basic experimental setup and results for the DF condition, which is performed to confirm the

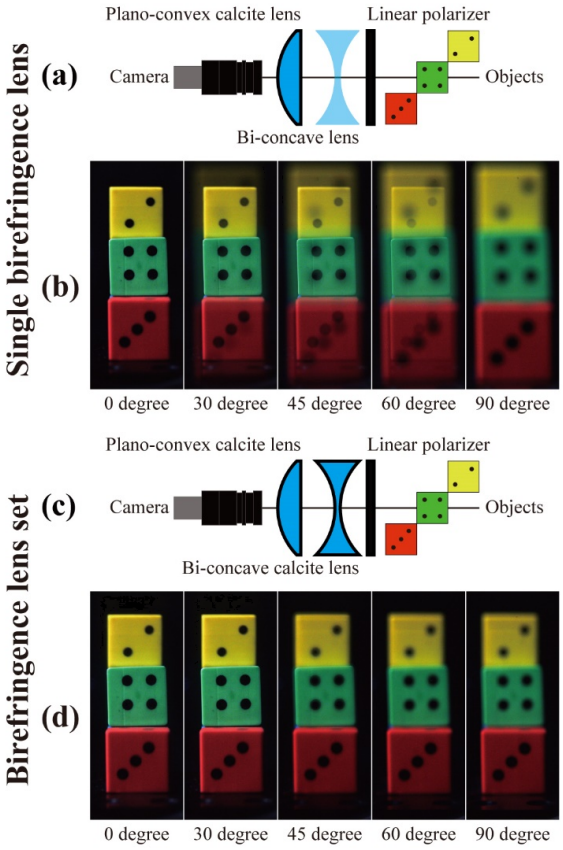

FIG. 3. Experiments for the DF condition: (a) and (b) respectively show the experimental setup and results using a single birefringent lens, while (c) and (d) show the experimental setup and results using the proposed birefringent lens set. The degree measures in (b) and (d) are the rotation angle of the linear polarizer.

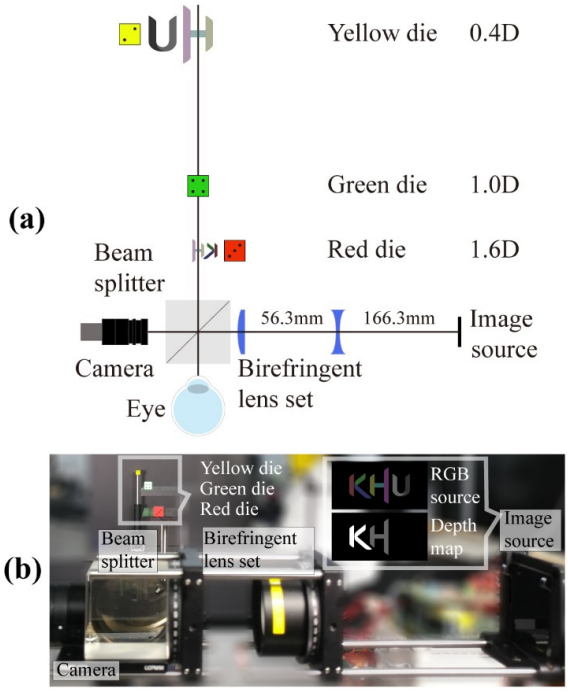

FIG. 4. The proposed DF-type 3D NED system: (a) schematic diagram of the experiment, (b) photograph of the experimental setup.

TABLE 2. Display-panel specifications

Pitch (μm)	Resolution (pixels) Height × Width	Size (mm)	Frame rate (Hz)
20.5	1400 × 1050	28.70 × 21.52	60

polarization characteristics of the birefringent lens set and its ability to provide a multifocal image in the proposed system. The setup of Fig. 3(a) shows the eyepiece using one birefringent convex lens. In this case, the focus and FOV of the eyepiece are changed by the incident polarization state, as shown in the results of Fig. 3(b), which are double-phase images and not suitable for the DF system. In addition, when replacing with a lens having each EFL equivalent to the birefringent lens in Fig. 3(a), a flat image corresponding to 0 or 90 degrees in Fig. 3(b) is displayed depending on the EFL. On the other hand, the designed eyepiece using two birefringent lenses shown in Fig. 3(c) can change the focus without varying the FOV. Therefore, the results shown in Fig. 3(d) present single-phase images just defocused depending on the polarization, which verifies the DF effect of the proposed eyepiece design.

Figure 4 shows the setup of the proposed system. The value of D_S is set to 166.3 mm and D_L is set to 56.5 mm, so that D_E and the depth range are 90.5 mm and 1875 mm respectively, the same as in the simulation. The eye relief of the implemented system is 20.5 mm, because a beam splitter having a thickness of 70 mm is included to display the represented images compare to real objects. The dice are placed with equal diopter spacing of 0.4 D (2500 mm), 1.0 D (1000 mm), and 1.6 D (625 mm), while the two image planes of the proposed eyepiece are located 0.4 D and 1.6 D from the eye respectively.

Table 2 shows the specifications of the display panel used as the image source in the proposed system. When the values of D_S and D_L set to DF conditions are fixed, the FOV_{DF} varies depending on W_S, and the diagonal length of the display panel is the same as the simulation condition of 35.9 mm.

IV. DISCUSSION

The accommodation range of the human eye is influenced by several factors, such as depth of focus depending on pupil diameter, luminance, contrast, and spatial frequency [19]. In this experiment, the accommodation range of the camera is set below ±0.3 D to distinguish the two image planes clearly.

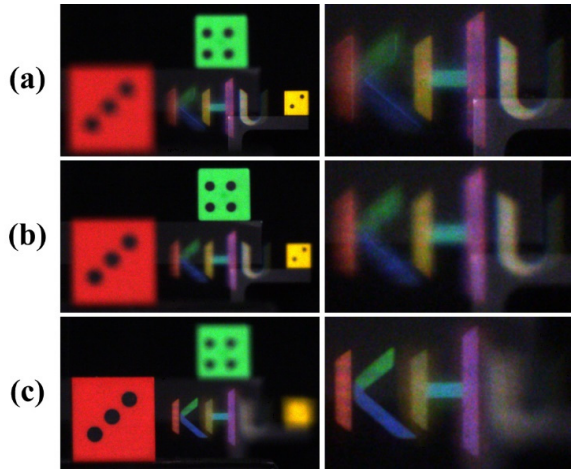

FIG. 5. Results of the experiment with accommodation cues: (a) focused on the yellow die (0.4 D), (b) focused on green die (1.0 D), and (c) focused on red die (1.6 D).

As shown in Fig. 5, the displayed image consists of multiple focal planes and is taken when the camera focuses on each die. Figure 5(a) is taken when the yellow die is in focus; only the letter U, at the same depth as the yellow die, appears clearly. In the case of the letter H, the part that occurs at 1.6 D is out of the accommodation range of the camera, and the other part that occurs at 0.4 D is clearly displayed, so it is combined and displayed as slightly blurred. Figure 5(b) is taken when the green die is in focus; all of the letters appear to be a little blurred, but when the accommodation range is expanded to above ±0.3 D, the letter H can be predicted to be expressed at an intermediate depth by the DF effect. Figure 5(c) is taken when the red die is in focus; only the letter K, at the same depth as the red die, appears clearly. In the case of the letter H, the part that occurs at 0.4 D is out of the accommodation range of the camera, and the other part that occurs at 1.6 D is clearly displayed, so it is combined and displayed as slightly blurred.

V. CONCLUSION

The proposed system, a DF-type 3D NED, has advantages such as a simple structure; a high-quality, high-resolution image resulting from not using time or spatial multiplexing schemes; and data depth less than a third of that for RGB data. Besides, the depth cues for not only accommodation but also vergence are present, for natural 3D image recognition. Therefore, the proposed system can be suitably applied for 3D AR/VR systems.

ACKNOWLEDGMENT

This research was supported by the MSIP (Ministry of Science, ICT and Future Planning), Korea, under the ITRC (Information Technology Research Center) support program (IITP-2019-2015-0-00448) supervised by the IITP (Institute for Information and communications Technology Promotion). We thank the Center for Imaging Media Research of the Korean Institute of Science and Technology for the use of their equipment.

REFERENCES

1. A. Maimone, A. Georgiou, and J. S. Kollin, "Holographic near-eye displays for virtual and augmented reality," ACM Trans. Graph. **36**, 86 (2017).
2. W. Cui and L. Gao, "Optical mapping near-eye three-dimensional display with correct focus cues," Opt. Lett. **42**, 2475-2478 (2017).
3. S.-B. Kim and J.-H. Park, "Optical see-through Maxwellian near-to-eye display with an enlarged eyebox," Opt. Lett. **43**, 767-770 (2018).
4. A. Maimone, D. Lanman, K. Rathinavel, K. Keller, D. Luebke, and H. Fuchs, "Pinlight displays: wide field of view augmented reality eyeglasses using defocused point light sources," ACM Trans. Graph. **33**, 20 (2014).
5. D. Dunn, C. Tippets, K. Torell, P. Kellnhofer, K. Aksit, P. Didyk, K. Myszkowski, D. Luebke, and H. Fuchs, "Wide field of view varifocal near-eye display using see-through deformable membrane mirrors," IEEE Trans. Vis. Comput. Graph. **23**, 1322-1331 (2017).
6. G.-A. Koulieris, B. Bui, M. S. Banks, and G. Drettakis, "Accommodation and comfort in head-mounted displays," ACM Trans. Graph. **36**, 87 (2017).
7. H. Hua, "Enabling focus cues in head-mounted displays," Proc. IEEE **105**, 805-824 (2017).
8. G. Kramida, "Resolving the vergence-accommodation conflict in head-mounted displays," IEEE Trans. Vis. Comput. Graph. **22**, 1912-1931 (2016).
9. S. Ravikumar, K. Akeley, and M. S. Banks, "Creating effective focus cues in multi-plane 3D displays," Opt. Express **19**, 20940-20952 (2011).
10. A. Tsunakawa, T. Soumiya, H. Yamamoto, and S. Suyama, "Perceived depth change of depth-fused 3-D display with changing distance between front and rear planes," IEICE Trans. Electron. **E96.C**, 1378-1383 (2013).
11. S.-G. Park, J.-H. Kim, and S.-W. Min, "Polarization distributed depth map for depth-fused three-dimensional display," Opt. Express **19**, 4316-4323 (2011).
12. S.-G. Park, S. Yoon, J. Yeom, H. Baek, S.-W. Min, and B. Lee, "Lamina 3D display: projection-type depth-fused display using polarization-encoded depth information," Opt. Express **22**, 26162-26172 (2014).
13. S. Yoon, H. Baek, S.-W. Min, S.-G. Park, M.-K. Park, S.-H. Yoo, H.-R. Kim, and B. Lee, "Implementation of active-type Lamina 3D display system," Opt. Express **23**, 15848-15856 (2015).

14. J.-Y. Hong, C.-K. Lee, S. Lee, B. Lee, D. Yoo, C. Jang, J. Kim, J. Jeong, and B. Lee, "See-through optical combiner for augmented reality head-mounted display: index-matched anisotropic crystal lens," Sci. Rep. **7**, 2753 (2017).
15. C. Yoo, K. Bang, C. Jang, D. Kim, C.-K. Lee, G. Sung, H.-S. Lee, and B. Lee, "Dual-focal waveguide see-through near-eye display with polarization-dependent lenses," Opt. Lett. **44**, 1920-1923 (2019).
16. G. D. Love, D. M. Hoffman, P. J. W. Hands, J. Gao, A. K. Kirby, and M. S. Banks, "High-speed switchable lens enables the development of a volumetric stereoscopic display," Opt. Express **17**, 15716-15725 (2009).
17. P. Jin, L. Gao, S. Zhu, and W. Qiao, "High-resolution head mounted display using stacked LCDs and birefringent lens," Proc. SPIE **10676**, 10671B (2018).
18. R. S. Eng and K. G. Leib, "Multiple Imagery with Birefringent Lenses," Appl. Opt. **8**, 2117-2120 (1969).
19. B. Wang and K. J. Ciuffreda, "Depth-of-focus of the human eye: theory and clinical implications," Surv. Ophthalmol. **51**, 75-85 (2006).